ALMA MEMO No. 451

SOME ERROR SOURCES FOR THE PWV AND PATH DELAY ESTIMATED FROM 183 GHZ RADIOMETRIC MEASUREMENTS AT CHAJNANTOR

Guillermo Delgado
Onsala Space Observatory / European Southern Observatory
Casilla 19001, Santiago 19, Chile
Email: gdelgado@eso.org

Fredrik T Rantakyrö
European Southern Observatory
Casilla 19001, Santiago 19, Chile
Email: frantaky@eso.org

Juan Pablo Pérez Beaupuits
European Southern Observatory
Casilla 19001, Santiago 19, Chile
Email: jperez@eso.org

Lars-Åke Nyman
Onsala Space Observatory / European Southern Observatory
Casilla 19001, Santiago 19, Chile
Email: lnyman@eso.org

Dedication

This ALMA memo is dedicated to Guillermo Delgado, who passed away last July. Guillermo provided a major contribution to the ALMA radiometric data analysis. He had taken a lead in the site testing campaign at Chajnantor as well as in the first steps for the site development. Until his last days he showed a keen interest and concern for the project. ALMA had become his life dream. Guillermo has also promoted the ALMA project at the Universities level in Santiago and thanks to him, several students are now connected to the radio-astronomy in Chile.

We are truly missing his support and enthusiasm.

D. Hofstadt

Abstract – We present here an extensive study of the accuracy of the determination of the PWV from antenna measurements and in the determination of the pathlength variations (and thus phase variations). The study focussed on the effects of instrument measurement effects and software issues. We have also investigated the effect of the water vapour scale height and the presence of water vapour layers in the determination of the path delay. After correcting the software for the instrumental effects and applying empirically determined corrections to the path delay estimates we reached a good agreement between observed path delay variations and the inferred path delay variations determined from the PWV measurements.

1   Introduction

We have noticed that there is a systematic tendency to obtain lower amplitudes for the phase variations obtained from radiometer data than those obtained with the interferometer [Delgado *et al.* 2000a and 2000b]. Although this amplitude difference does not affect the result of the correlation of the signals, it does affect the residual of the phase correction achieved by subtracting the radiometer determined phase noise from the interferometer measured phase noise.

Here we describe and quantify a series of error sources that ought to be the most relevant ones. These include the hardware of the interferometer (load calibrations), the determination of the PWV from the antenna temperature values (using an atmospheric water line model), and the determination of the pathlength variations starting from PWV values.

Of fundamental importance is the effect of the atmospheric water line model in use and its sensitivity to measured quantities. Thus we have focussed this study on understanding the sensitivity of the model [Waters, 1976] to the most relevant quantities that for Chajnantor are not fully known or are known to vary. Two of these quantities are the scale height for the water vapour distribution and the presence of water vapour layers.

Normally it is assumed that the water vapour has an exponential distribution with a scale height in the range of 1 to 2 km. Most of the literature assumes a value of 2 km for this parameter [*e.g.* Thompson *et al.*, 1994]. We have found that water vapour density profiles obtained from radiosonde launches made at Chajnantor yields a slightly lower value of 1.5 km for the water vapour scale height. There are also daily scale height variations seen in the radiosonde data, something that we will explore in depth in a future ALMA Memo.

The atmosphere at Chajnantor, just like everywhere else, is not ideal and the water vapour distribution is an approximation to an exponential distribution. The main deviation from the ideal distribution is occasional presence of an inversion layer trapping the water vapour. As we cannot currently measure the possible presence and altitude in real-time of the inversion layers we have chosen not to include the inversion layer in our software model. We evaluated the sensitivity of the model to this parameter to assess the loss of accuracy in the path length determinations introduced by assuming an ideal atmosphere.

2   Load Calibration

The estimation of the amount of PWV at each radiometer is done from the antenna temperature values. Thus it is important to have a properly calibrated antenna temperature to assure an accurate input to the atmospheric model. In addition, since the phase variation is calculated as a differential measurement between two different instruments then we must fully understand the instrumental error introduced by a calibration difference in the two instruments.

The total radiation coming to the WVR is detected by each IF channel within the specific channel bandwidth of each one of these bands. The power is detected after down-conversion, and a voltage-to-frequency (V/F) conversion. To obtain a calibrated antenna temperature T_a, from the total power measurements in the radiometer, we look consecutively to the sky and the two calibration loads (one "warm" at about +40°C and the other "hot" at about +100°C). The response to these measurements is used to calibrate the antenna temperature through:

$$T_a = \frac{\left(IF_{sky} - IF_{warm}\right)T_{hot} + \left(IF_{hot} - IF_{sky}\right)T_{warm}}{IF_{hot} - IF_{warm}} \qquad (1)$$

Where T_{hot} and T_{warm} are the physical temperatures measured at the calibration loads, and IF_i is the response of the radiometer (in arbitrary units) to the different inputs.

Because the calibration loads are not perfect blackbodies and the presence of mechanical misalignments, the physical temperature is not equal to the radiometric temperature. In order for (1) to give the right value for the antenna temperature we should use the brightness temperature of the loads instead of their actual physical temperature. These radiometric temperatures are obtained after a calibration with loads of known temperature. Any residual difference after the calibration will produce an error in the measured PWV variations.

2.1 Calibration of the loads

To calibrate the loads in order to obtain the actual value of the radiometric temperature as function of its physical temperature, we have to observe at least two loads of known value. These loads should fill completely the beam of the radiometer.

The usual method is to measure the response of the radiometer to a piece of Eccosorb® at ambient temperature and the response to a piece of Eccosorb® soaked in liquid nitrogen.

If we have measured the response of the radiometer to a liquid nitrogen load, an ambient temperature load, and one of the two calibration loads, we have a set of three equations:

$$IF_{load} = K\left(T_{sys} + T_{load}\right)$$
$$IF_{N_2} = K\left(T_{sys} + T_{N_2}\right)$$
$$IF_{amb} = K\left(T_{sys} + T_{amb}\right)$$

(2)

Where IF_{load} is the V/F converter response in arbitrary units to a brightness temperature T_{load} of the load, in a channel with conversion gain K and system temperature T_{sys}. In the same way, IF_{N2} and IF_{amb} are the response to loads at temperatures of T_{N2} and T_{amb}.

Solving the system of equations (2) for T_{load}, we obtain:

$$T_{load} = \frac{\left(IF_{load} - IF_{N_2}\right)T_{amb} + \left(IF_{amb} - IF_{load}\right)T_{N_2}}{IF_{amb} - IF_{N_2}}$$

(3)

Ideally one performs the ambient temperature and liquid nitrogen temperature measurements at the same time to guarantee that the value of T_{sys} and K remain unchanged during the measurement time.

During September 2000 the two WVR that normally are located at the ends of a 300-m baseline were moved together and a side-by-side test was done with the two WVR looking the same sky position. During this time a series of measurements of liquid N_2 and ambient temperature loads were done.

From the weather station the ambient temperature at the time of the measurements was -2° C, thus we assume that the Eccosorb® load was at thermal equilibrium with $T_{amb} \approx 271$ K.

To obtain the boiling point of liquid nitrogen at Chajnantor we use the Claussius-Clapeyron equation, with the assumption that the change in volume upon vaporisation equals the ideal-gas volume of the vapour. This leads to the equation:

$$\frac{\Delta t}{\Delta p} = \frac{R t_b^2}{p_0 \Delta_{vap} H(t_b)}$$

(4)

Where R is the molar gas constant (8.31451 J/mol/K), p_0 is the normal pressure (1013.25 mbar), t_b the normal boiling point referred to the normal pressure (77.36 K for N_2), and $\Delta_{vap}H(t_b)$ the heat of vaporisation for N_2 (5.57·10³ J/mol). Replacing all the constants, we have:

$$\frac{\Delta t}{\Delta p} = 8.816532 \cdot 10^{-3} \qquad [K/mbar]$$

(5)

The change in pressure Δp from the standard atmosphere, using a pressure value for Chajnantor of 553 mbar, is 460 mbar. Hence the boiling point of N_2 at the height of Chajnantor is $T_{N2} = 73.3$ K. Since the Eccosorb® soaked in nitrogen is not a perfect blackbody we can assume that its effective temperature is about 5 K over the boiling point of nitrogen, thus in our calculations we will use a value of $T_{N2} \approx 78$ K.

Table 1. Physical and radiometric temperatures for both WVR and the scaling factor between them.

	East radiometer	West radiometer
Hot load physical temperature [K]	372.7	373.1
Hot load radiometric temperature [K]	365.1	367.0
Radiometric/physical	0.980	0.982
Warm load physical temperature[K]	303.0	308.1
Warm load radiometric temperature [K]	297.43	305.1
Radiometric/physical	0.984	0.990

Figure 1 shows the PWV during a complete day as measured by each radiometer (09/09/00). The left plot gives the PWV before applying the calibration to the loads; this is using the physical temperatures on equation (1). The right plot shows the same data with the load correction shown on Table 1. The improvement is evident.

Figure 2 shows the correlation between the PWV obtained with each WVR observing to the zenith on a side-by-side comparison during the 09/09/00 before and after the calibration of the loads. The PWV range during this 24-hour observation was between ~0.6 to ~2.2 mm.

Figure 3 shows the ratio between the PWV measured by the West and the East WVR. The ratio before calibration has an average of 0.93 and after the calibration this ratio is of 1.03.

3   Relation between pathlength variation and PWV

The excess propagation path (or path delay) refers to the extra path traversed by an electromagnetic wave travelling through a media as compared with the same wave travelling through vacuum. The extra path is due to the time delay introduced by the reduced phase velocity in the physical media as compared with free-space. This pathlength is directly related to the refractivity N of the transmission media by the relation [Thompson *et al.*, 1986]:

$$L(s) = 10^{-6} \int_0^s N(s)\,ds \qquad (6)$$

The refractivity in the atmosphere can be divided in a component due to the presence of water vapour and another component due to all the other gaseous components of the atmosphere (the "dry" component). A common expression for the refractivity N is given by [Elgered, 1993]

$$N = k_1 \frac{e_d}{T} Z_d^{-1} + k_2 \frac{e_w}{T} Z_w^{-1} + k_3 \frac{e_w}{T^2} Z_w^{-1} \qquad (7)$$

Where e_d is the partial pressure of the "dry" component of the atmosphere in mbar, e_w is the partial pressure of the water vapour (*i.e.* the total atmospheric pressure $P = e_d + e_w$), k_i are experimentally determined constants, T is the atmosphere temperature, and Z_d^{-1} and Z_w^{-1} are the inverse compressibility factors for dry air and the water vapour respectively (correction to the departure from the ideal gas law).

Under normal conditions in the terrestrial atmosphere, the compressibility factors deviate from unity by less than 1 part in 10^3 [Buck, 1981], so they can safely be discarded on the calculations done here.

For the experimental factors k_i there are many sets of values in the literature. Here we will use the ones given by [Thompson *et al.*, 1986]

$$N = 77.6\frac{e_d}{T} + 64.8\frac{e_w}{T} + 3.776 \cdot 10^5 \frac{e_w}{T^2} \qquad (8)$$

Using the equation of state for an ideal gas and replacing all the constants, we obtain:

$$N = 0.2228\rho_d + \left(0.299 + 1742.2\frac{1}{T}\right)\rho_w \qquad (9)$$

With densities expressed in gr/m^3.

The first term corresponds to the path delay introduced by the "dry" atmosphere that, under normal conditions in the zenith direction at Chajnantor, is of the order of 1 m. Here we are not interested in the slowly varying contribution, but rather in the "wet" part of the refractivity that depends on the water vapour density. Hence the pathlength variations are given by the integral of the second term (the "wet" term) according to (9)

$$L_w(\rho_W, T) = 0.299 \cdot 10^{-6} \int_0^\infty \rho_w \, ds + 1742.2 \cdot 10^{-6} \int_0^\infty \frac{\rho_w}{T} \, ds \qquad (10)$$

The first integral is by definition; the PWV contained in the column along the integration path. Thus,

$$L_w(\rho_W, T) = 0.299 \, PWV + 1742.2 \cdot 10^{-6} \int_0^\infty \frac{\rho_w}{T} \, ds \qquad (11)$$

If equation (11) is solved for an isothermal atmosphere at 280 K the relation between PWV and pathlength becomes $L_W = 6.52 \, PWV$. This value is in agreement with radiosonde measurements done by [Hogg *et al.*, 1981] where they obtain, for a location in California close to sea level, a value of 6.5 mm of extra path delay due to each mm of PWV.

Assuming for Chajnantor an isothermal atmosphere at 269 K [Paine et al., 2000], we obtain an approximated relation between PWV and wet path delay of

$$L_w(\rho_W, T) = 6.776 \, PWV \qquad (12)$$

Relation (12) is valid for Chajnantor and should be compared with the value of $L_W = 6.3 \, PWV$ given by [Thompson *et al.*, 1986] and which was used in our data reduction software. The new values give pathlengths that are of the order of 8 % smaller and, thus 8 % smaller phase variation amplitudes.

We should stress that in much of the literature, including [Thompson *et al.*, 1986], the refractivity given in (9) is arranged to have the first term expressed in terms of the total atmospheric pressure. This means that this component will also have some dependence on the water vapour (the total atmospheric pressure $P = e_d + e_w$). This approach is valid when we want to calculate the total path delay ("dry" and "wet" components) and the required accuracy is within the accuracy of the barometer used to measure the atmospheric pressure. In our case, we need an accurate measurement of the path delay variations due to the fast varying "wet" component, not considering the "dry" component that, at the measurement time scale, is almost constant. Thus, we should use equation (11).

4   Water vapour line model

In non-scattering media the radiative transfer equation solves, for an isothermal medium in local thermodynamic equilibrium in the Raleigh-Jean regime, as:

$$T_b(\tau_v) = T_{bg} \, e^{-\tau_v} + T_{atm} \left(1 - e^{-\tau_v}\right) \qquad (13)$$

Where T_{bg} is the cosmic background temperature (2.7 K), T_{atm} is the equivalent blackbody temperature of the atmosphere [K], and τ_ν is the opacity or optical depth depending on the observation frequency and elevation angle.

In our case, at 183 GHz, the cosmic background temperature is too low to hold the Raleigh-Jeans condition so the equivalent blackbody temperature of the cosmic background must be used resulting in:

$$T_b(\tau_\nu) = T_{atm}\left(1 - e^{-\tau_\nu}\right) + \frac{h\nu}{k}\frac{1}{e^{h\nu/kT_{bg}} - 1}e^{-\tau_\nu} \qquad (14)$$

With h is the Planck's constant ($6.626076 \cdot 10^{-34}$ [Js]) and k is the Boltzmann's constant ($1.38066 \cdot 10^{-23}$ [J/K]).

The radiometer response, as for all real optical systems, has some losses and the radiometer will not couple with 100% efficiency to the sky. In general, the response of a radiometer, called antenna temperature, is given by

$$T_A(\tau_\nu) = \eta\, T_b(\tau_\nu) + T_{amb}(1 - \eta) \qquad (15)$$

Where η is the coupling efficiency to the sky. The second term of (15) represents the radiation pick-up from the sidelobes and corresponds mainly to radiation at ambient temperature.

From equation (15) we know a priori only the coupling efficiency (measured by performing sky scans [Delgado et al., 1999]) and the ambient temperature (measured by the weather stations). The brightness temperature of the atmosphere, according to (14), depends on the equivalent blackbody temperature of the atmosphere and the opacity τ_ν.

At the frequencies around the 183 GHz water line in the model developed by [Waters, 1976], τ_ν is then a function mainly of the water vapour content in the atmosphere (water vapour density) and the physical conditions of the atmosphere (pressure and temperature). We can thus disregard any other molecules present in the atmosphere. The opacity than has a term corresponding to the discrete energy transitions of the water molecule plus an empirical term accounting for other contributions not properly understood in this model (most probably the far wings of infrared emission lines of water vapour).

The line shape depends on the local pressure, temperature and density of the water vapour, through a non-linear relation.

The water vapour density at the surface can be estimated starting from meteorological variables [Reber and Swope., 1972 and Butler, 1998]. Using these values as a starting point for a water vapour distribution we can define a water vapour density distribution as function of height. If the atmosphere is divided in conveniently sized layers, we can assume isothermal layers and thus the equivalent blackbody temperature of each layer can be assumed to be the same as the physical temperature of that layer. We can use the temperature and pressure distribution models as function of height and assign a fixed temperature and pressure value to each atmosphere layer.

In our computations we have used a more efficient method to determine the water vapour density at the surface by using the temperature of the channel at 7.6 GHz from the line centre [Delgado *et al.*, 1999] as a first guess of the PWV content. Then, assuming an exponential distribution of the water vapour density, we obtain the ground value by inverting the integral relation for the PWV (equation (16)).

The integrations needed in all our calculations are replaced by discrete sums over discrete lengths of atmosphere through the layers, all considered under isothermal and isobaric conditions.

When we observe with the 183 GHz radiometers at Chajnantor, we obtain the value for $T_A(\tau_\nu)$ at three different channels close to the 183 GHz line centre [Delgado *et al.*, 1999, 2000a]. Comparing the outcome of the water line model and iterating on the water vapour density, we obtain a best-fitting value for the water vapour density. Integrating this water vapour density along the observation path we can estimate the amount of water vapour along this atmospheric column using:

$$PWV = 10^{-6}\int_0^s \rho_0\, e^{-s/h_0}\, ds \qquad (16)$$

Where h_0 is the scale height factor for the water vapour distribution. This value can be found often as 2 km in the literature, but measurements at Chajnantor with radiosonde based measurements show that an average value of about 1.5 km is a more realistic value.

In our previous work [Delgado *et al.*, 1999, 2000a, 2000b] we estimated the 183 GHz line shape and intensity using the model by Waters (1976). The following sections evaluate the accuracy of the PWV due to different parameters and finally we make a comparison of the Waters model with the one by Pardo et al. (2001).

4.1 Response of the WVR to different PWV levels

We have used equation (15) in conjunction with equation (14), to define a "standard" atmosphere at Chajnantor, with real parameters for the radiometer. The standard atmosphere is defined as one with a ground temperature of 273.16 K, ground pressure of 558 mbar, starting integration height 5.0 km, ending integration height 8.0 km (total zenith column 3.0 km), scale height for the water vapour distribution 1.5 km, and a 1 mm precipitable water vapour column in the zenith direction. For the radiometer we included a coupling efficiency of 0.97 representative of the WEST radiometer [Delgado et al., 1999].

The result of varying the amount of PWV on the 183 GHz line profile is seen on Figure 4 for the case of 5, 1 and 0.3 mm of PWV.

Note: The only remark here is about the saturation of the water line due to an increase of the opacity for PWV contents over 2 mm. This is due to the line becomes optically thick close to the line centre and thus we measure the equivalent blackbody temperature of the atmosphere (T_{atm} in equation (16)). From the simulation of the line under a 5 mm of PWV condition we have saturation at 268 K, very close to the value estimated by [Paine et al., 2000] for an isothermal atmosphere of 269 K for Chajnantor. This value, for the equivalent blackbody temperature of the atmosphere, depends on the ground temperature and thus can be considered only as a reference under the "standard" atmosphere condition for Chajnantor.

4.2 Line shape and intensity for different integration heights for the water column

In our calculations we are using a maximum height of 8 km for the integration, giving an integration column of 3 km. Due to the exponential dependence of water vapour, with a scale height of 1.5 km, the water vapour density at 3 km over the site is about 14% of the ground value. In principle we can integrate to any value within the troposphere and we evaluate here this dependence.

In Figure 5 (left plot) we have the line shape and intensity of a line under "standard" conditions for a 3-km column (integration up to 8 km) and a 15-km column (integration up to 20 km). The shape does not change too much in the two cases, but the intensity is higher in the case of the larger integration column. In the same figure (right plot) we have the ratio between the two line shapes, showing that at the centre the relative intensity differs by less than 2% between the two integration columns. The worst case difference (about 4.7 GHz from the line centre) is about 3% and is very close to the WVR channel at 4.2 GHz from the line centre.

4.3 Line shape and intensity of different scale heights for the water vapour density distribution

By combining equations (14) and (15), and obtaining the PWV from equation (16) it is necessary to use the water vapour scale height for the assumed exponential distribution. We know from radiosonde profiles at Chajnantor that the average scale height is close to 1.5 km with variations that seem to follow a daily cycle (this will be the subject of a future ALMA Memo). Here we estimate the sensitivity of the calculated line shape for an "standard" atmosphere in Chajnantor, varying only the scale height between 1 and 2 km.

In Figure 6 (left plot) we have the line shape for the two extreme cases, here we see that both lines are almost identical. In the same figure (right plot) we have the ratio between the intensity of the line for the two considered cases, showing that at the line centre the relative amplitude difference is less than 1%, while again at 4.7 GHz the relative amplitude difference is maximum but less than 2%.

4.4 Line shape and intensity under the presence of water vapour layers

Using an exponential water vapour distribution is a very strong simplification of real atmosphere above Chajnantor. We know from radiosonde measurements that quite often there are inversion layers over

Chajnantor trapping some of the water vapour. The number of layers, their relative intensity and their height are highly variable during the day.

Here we evaluate the line shape and intensity of the simulated line under a "non-standard" atmosphere in Chajnantor, distributing the 1-mm of precipitable water vapour between the "standard" column and an inversion layer.

Figure 7 (left plot) shows the line shape for the simple case of an exponential distribution with no layer of water and the case when 25% of the water in the atmospheric column is trapped in a layer at 500 m (70% of the time the layers are below 1000 m according to [Delgado et al., 2001]. As expected, the case with a layer of water vapour have a larger amplitude and broader wings, compared with the case of no layer, because more water will be at a higher temperature and pressure. In Figure 7 (right plot) the ratio between the two cases is shown and it can be seen that at the centre the relative difference is about 2%, while at about 3 GHz from the line centre the relative difference achieves a maximum of about 4%.

4.5 Line shape and intensity of the Waters model compared with the model of Pardo et al.

There have been some questions about the accuracy of the Waters model that we are using in our data reduction programs. The model is used to retrieve the line profile that is then fitted to the measured antenna temperature values Waters (1976) and [Delgado et al., 1999, 2000, 2001].

The model used is the one proposed by Waters (1976) and it is based on the works by Liebe (1976). Recently Pardo et al. (2001) has presented an atmospheric transmission model that is claimed to have a better agreement with measured values. The main difference between this new model and the traditional ones lies in the inclusion of lines over 1 THz, inclusion of Ozone and other minor components, a better treatment of the dry continuum and H_2O excess pseudocontinuum terms and comparison with measured data, and a better parameterisation of the resonant absorption.

In Figure 8 we present a direct comparison between the outcome of Pardo and Waters model. It can be seen that the line-shape close to the centre is very similar in both models, starting a departure at about ± 2 GHz around the line centre. In the worst case (0.3 mm of PWV) the average ratio between the models for the upper and lower side bands is of 0.83 for the 4.1 GHz IF and 0.73 for the 7.6 GHz IF.

In the case of 1.0 mm of PWV, also the centre channel is almost identical in both models, with the average ratio between the models for the upper and lower side bands is of 0.91 for the 4.1 GHz IF and 0.83 for the 7.6 GHz IF. The main difference is in the continuum level, higher in Pardo's model as compared with Waters. This is expected as Pardo´s model takes into account the dry continuum and as we have discussed in Section 2 this dry continuum is not considered in the Waters model. At 183 GHz the dry continuum is increasing with frequency and thus causes the larger difference for the 7.6 GHz IF.

5   Calculation of the Precipitable Water Vapour

According to equation (16) the PWV is obtained from an integration of the water vapour density. If an exponential distribution for the water vapour is assumed and the integration is performed from the ground to a height h, equation (16) can be integrated directly as:

$$PWV = 10^{-6} \int_0^h \rho_0 \, e^{-s/h_0} \, ds = \rho_0 \, h_0 \left(1 - e^{-h/h_0}\right) 10^{-6} \qquad (17)$$

The water vapour density ρ_0 is obtained in the data reduction software from the best-fitting value using the Waters atmospheric water line model and the measured antenna temperature [Delgado et al., 1999, 2000].

If the integration in equation (17) is performed to infinity, the PWV can be expressed as:

$$PWV = \rho_0 \, h_0 \, 10^{-6} \qquad (18)$$

In the data reduction programs that we have been using so far to calculate the PWV at Chajnantor and in the phase correction experiments [Delgado *et al.* 2000a and 2000b] we have used equation (18) to calculate the PWV using $h_0 = 1.5$ km and $h = 3$ km, thus:

$$PWV = 0.86 \, \rho_0 \, h_0 \, 10^{-6} \qquad (19)$$

Thus the calculations of PWV that we have performed in the last two years are only an 86% of the PWV value that correspond to the obtained water vapour density at ground level and an infinite integration column. This factor translates also to phase variation amplitudes that are 14% smaller than what they should be for a given PWV.

6 Conclusions

We have analysed how several instrumental effects, atmospheric model details, and, software issues are affecting our estimate of the PWV and the pathlength derived from PWV or water vapour density.

The main finding is that in the data reduction software the PWV has been systematically calculated 14% lower than the value that should have been obtained considering an infinite column over Chajnantor. This can be translated linearly to the pathlength variations and thus phase variations calculated from the PWV.

Also we demonstrated that the linear relation between pathlength variations and PWV variations used by us ($L_w = 6.3$ PWV) was giving 8% lower values that what it should give for Chajnantor, considering the effective atmospheric temperature at Chajnantor and a relation that considers the full affect of PWV over the pathlength variation ($L_w = 6.776$ PWV).

We have also studied the problem of the relative calibration of the two radiometers. The error is not significant and was further reduced by load calibration performed using liquid nitrogen and ambient temperature loads on both radiometers.

Exploring the water line model that we are using [Waters, 1976], we estimated its sensitivity to relevant parameters (integration height, water vapour scale height, water vapour layers). It was found that the final model is accurate to within 3%. If this is extrapolated to phase variations (something that can not be done directly, but just as an estimation), we have phase variation estimates accurate to within 3%.

From radiosonde measurements the water vapour scale height is known to vary during the day, this will be explored in a future ALMA Memo. Also, from the same radiosonde measurements, we know that the presence of water vapour layers over Chajnantor is something frequent during daytime. The effect of the water vapour layers is the largest one on the explored parameters, it is of the order of 2% to 4% depending on the IF channel, for a water vapour layer trapping 25% of the water vapour at 500 m. The problem with the water vapour layers is that we can not take them into account during the data reduction because we do not have a real-time measurement of the water vapour layers.

Also we compared the atmospheric water line model that we are using (Waters 1976) against a newer model [Pardo, 2001]. The line intensity is the same with both models; the main difference is in the continuum level, higher in Pardo's model compared with Waters. This introduces a difference in the two outer IF channels, which are higher for lower PWV values. With the average ratio between the models for the upper and lower side bands for 0.3 mm of PWV being of 0.83 for the 4.1 GHz IF and 0.73 for the 7.6 GHz IF

If we consider an error of about 3% for possible water vapour layers, variation of the water vapour scale height, etc. and add the other errors obtained (error on the absolute value of PWV and error on the path length determination from PWV), we conclude that the phase variation, determined from the radiometer data was underestimated by 22%.

The main error sources, accounting for a phase amplitude error of 25%, have already being corrected in the data reduction software. The smaller 3% average error can not be controlled at the moment.

7   References

A. Buck, "New Equations for Computing Vapor Pressure and Enhancement Factor," J. App. Met., Vol. No. 20, pp. 1527-1532, 1981.

B. Butler, "Precipitable Water at the VLA –1990-1998," ALMA Memo Series No. 237, 1998.

G. Delgado, A. Otárola, V. Belitsky, D. Urbain, and P. Martin-Cocher, "The Determination of Precipitable Water Vapour at Llano de Chajnantor from Observations of the 183 GHz Water Vapour Line," ALMA Memo Series No. 271, 1999.

G. Delgado, A. Otárola, L-Å. Nyman, R. Booth, V. Belitsky, D. Urbain, R. Hills, Y. Robson, and P. Martin-Cocher, "Phase Correction of Interferometer Data at Mauna Kea and Chajnantor," ALMA Memo Series No. 332, 2000a.

G. Delgado, L-Å. Nyman, A. Otárola, R. Hills, and Y. Robson, "Phase Cross-correlation of a 11.2 GHz Interferometer and 183 GHz Water Line Radiometers at Chajnantor," ALMA Memo Series No. 361, 2000b.

G. Delgado and L-Å. Nyman, "Velocity of the Effective Turbulence Layer at Chajnantor Estimated from 183 GHz Measurements," ALMA Memo Series No. 363, 2001.

G. Elgered, "Tropospheric radio-path delay from ground based microwave radiometry," in M. Janssen (Ed.), *Atmospheric Remote Sensing by Microwave Radiometry*, John Wiley & Sons, Inc., 1993.

D. Hogg, F. Guirand, and M. Decker, "Measurement of Excess Radio Transmission on Earth-space Paths," Astron. Astrophys., Vol. 95, pp. 304-307, 1981.

S. Paine, R. Blundell, D. Cosmo Papa, J.W. Barnett, S. Radford, 2000, PASP, Vol 112, p108

J. Pardo, J. Cernicharo, and E. Serabyn, "Atmospheric Transmission at Microwaves (ATM): an Improved Model for mm/submm Applications," IEEE Trans. Ant. Prop., Vol. 49, No 12, Dec 2001.

E. Reber and J. Swope, "On the Correlation of the Total Precipitable Water in a Vertical Column and Absolute Humidity at the Surface," J. Appl. Met., No. 11, pp. 1322-1325, 1972.

A. Thompson, J. Moran, and G. Swenson, *Interferometry and Systhesis in Radio Astronomy*, Krieger Publishing Company, 1994.

J. Waters, "Absorption and emission by atmospheric gases," in *Methods of Experimental Physics*, M. Janssen (Ed.), Vol. 12B, pp. 142-176, 1976.
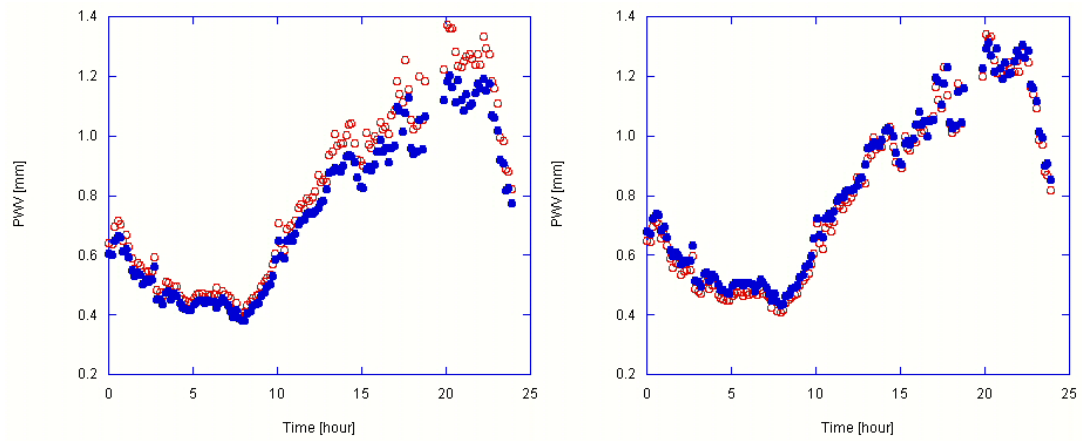
Figure 1. PWV time series for the WVR during day 09/09/00. The plot to the left is before the load calibration and the plot to the right is after the load calibration.
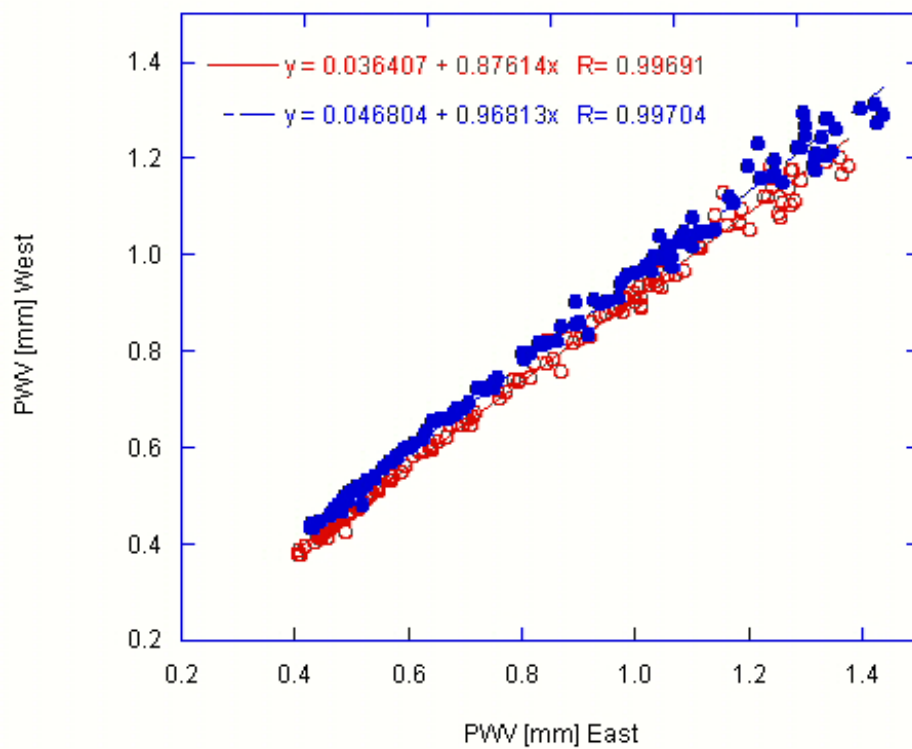

Figure 2. Correlation of the PWV time series for the WVR during day 09/09/00. The red circles represent the response before the load calibration and the blue solid dots represent the response after the load calibration.
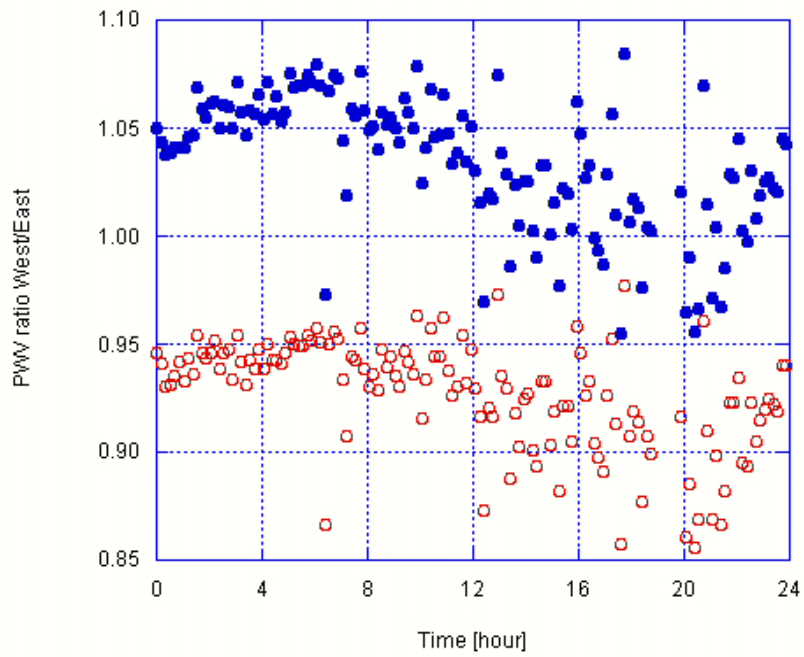
Figure 3. Ratio between the West and East radiometer PWV measurement during day 09/09/00. The red circles represent the response before the load calibration and the blue solid dots represent the response after the load calibration.
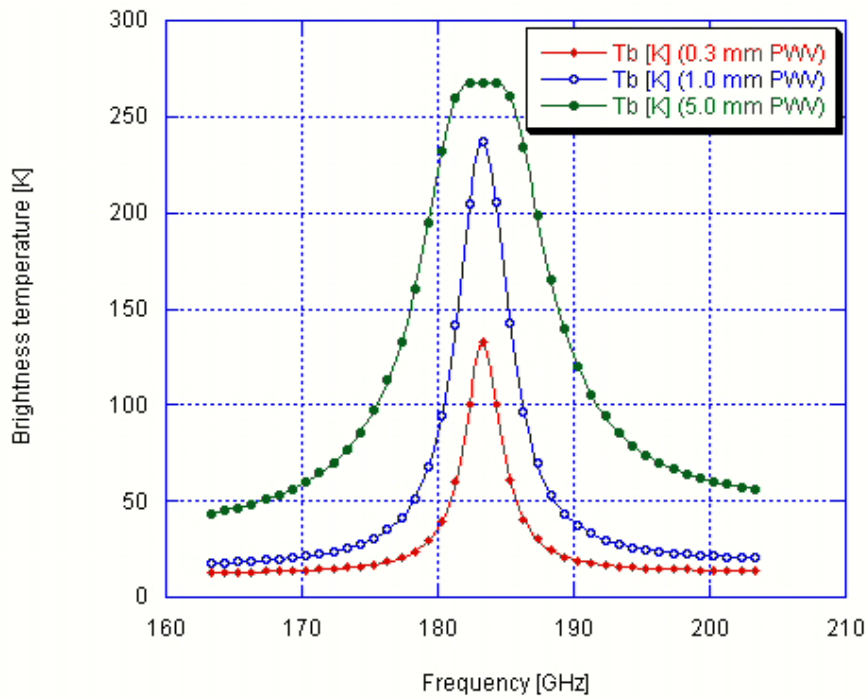

Figure 4. 183 GHz water line simulations for 0.3 mm (red curve), 1 mm (blue curve), and 5 mm (green curve) of PWV.
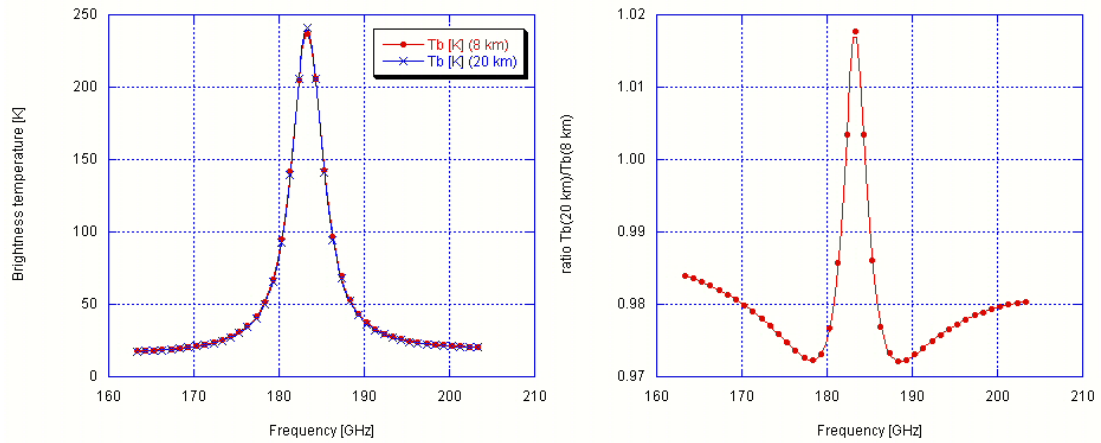
Figure 5. 183 GHz water line sensitivity to the height of the integration column (left), the filled dots are for a 3-km column over the site and the blue crosses are for a 15-km column. The right plot shows the ratio between the two lines.
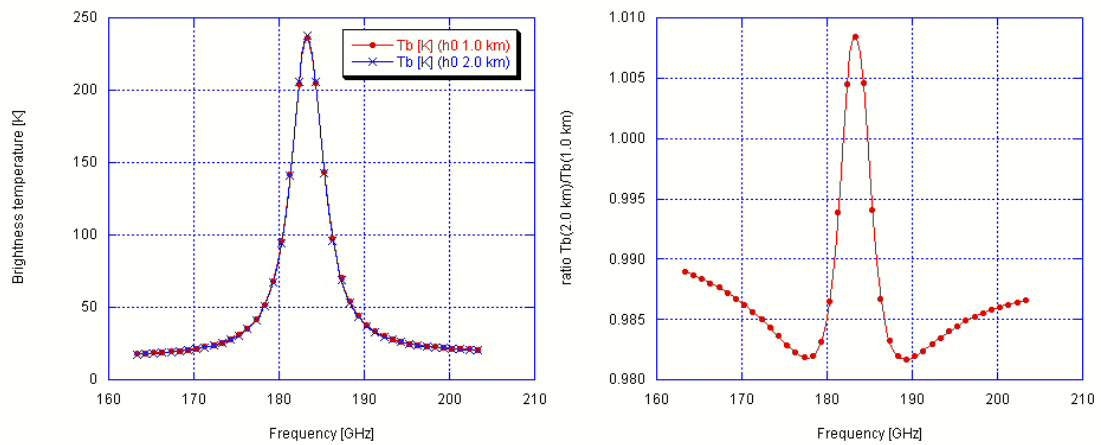
Figure 6. 183 GHz water line sensitivity to the scale height of the water vapour distribution (left), the filled dots are for a 1-km scale height and the blue crosses are for 2-km scale height. The right plot shows the ratio between the two lines.
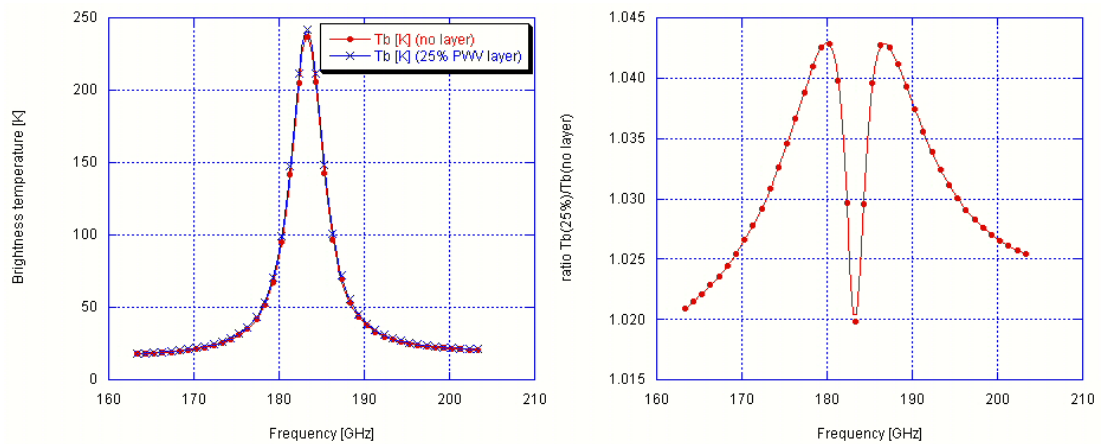
Figure 7. 183 GHz water line sensitivity to the presence of a water layer (left), the filled dots are for the case when no-layer is present and the blue crosses are for the case when 25% of the water is trapped on a layer at 500 m over the site. The right plot shows the ratio between the two lines.
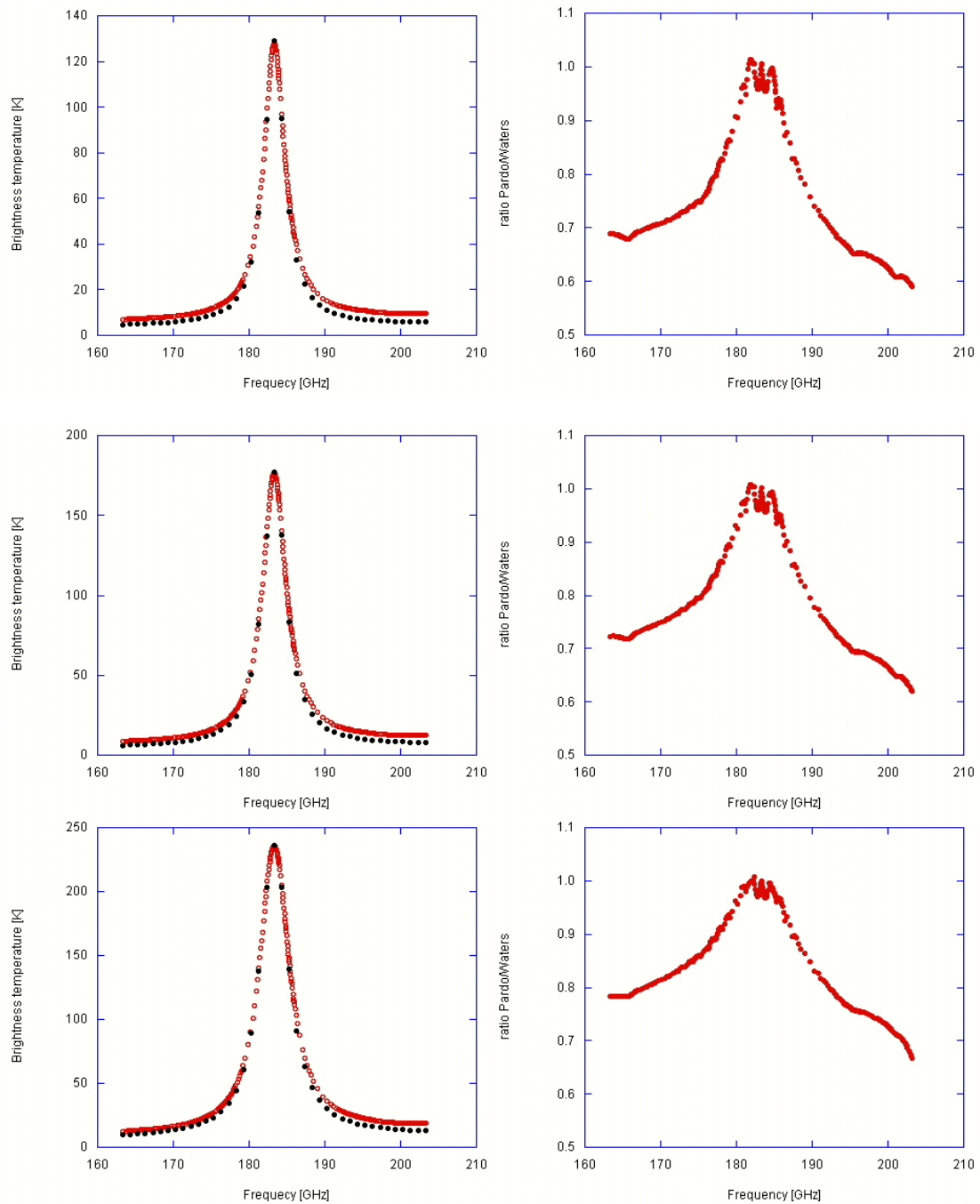
Figure 8. Comparison between Waters's model [Waters, 1976] and Pardo's model [Pardo *et al*., 2001]. The left plots show the direct comparison, with the solid black dots corresponding to Waters's model and the red open dots are Pardo's model. The right plot is the ratio between the value given by Pardo over the value given by Waters. From top to bottom we have 0.3, 05, and 1.0 mm of PWV, the rest of the parameters being those of a "standard" atmosphere at Chajnantor (see text for details).